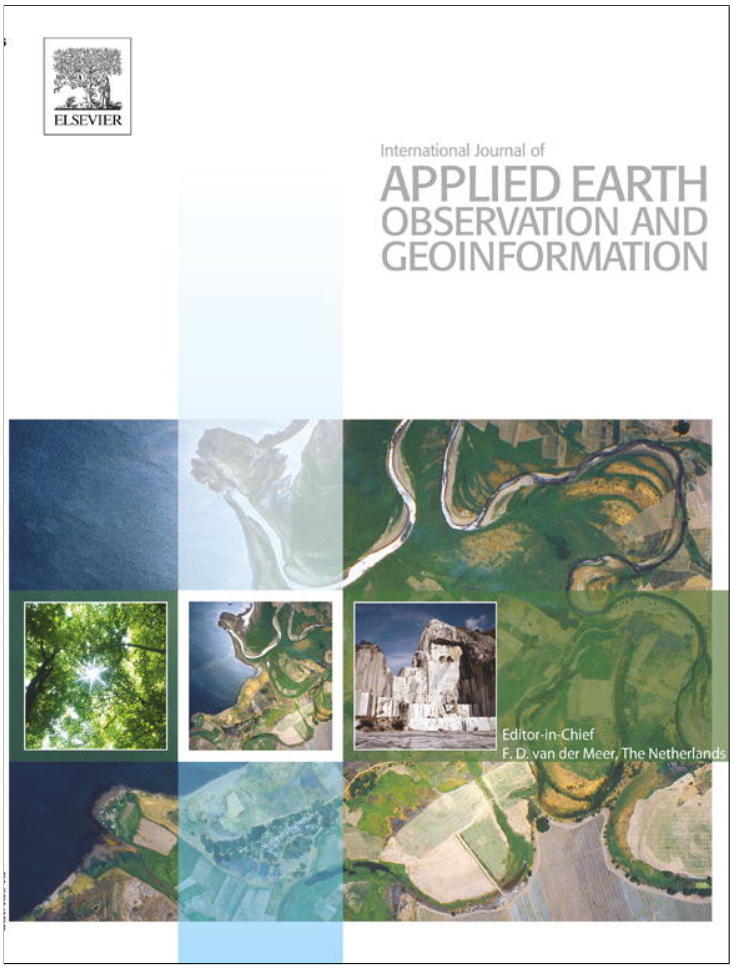

International Journal of Applied Earth Observation and Geoinformation 26 (2014) 12–20

Contents lists available at SciVerse ScienceDirect

International Journal of Applied Earth Observation and Geoinformation

journal homepage: www.elsevier.com/locate/jag

Inversion of the PROSAIL model to estimate leaf area index of maize, potato, and sunflower fields from unmanned aerial vehicle hyperspectral data

Si-Bo Duan[a,b,c], Zhao-Liang Li[d,c,*], Hua Wu[a], Bo-Hui Tang[a], Lingling Ma[e], Enyu Zhao[e,b], Chuanrong Li[e]

[a] State Key Laboratory of Resources and Environment Information System, Institute of Geographic Sciences and Natural Resources Research, Chinese Academy of Sciences, Beijing 100101, China
[b] University of Chinese Academy of Sciences, Beijing 100049, China
[c] ICube, UdS, CNRS, 300 Bld Sebastien Brant, BP10413, 67412 Illkirch, France
[d] Key Laboratory of Agri-informatics, Ministry of Agriculture/Institute of Agricultural Resources and Regional Planning, Chinese Academy of Agricultural Sciences, Beijing 100081, China
[e] Academy of Opto-Electronics, Chinese Academy of Sciences, Beijing 100080, China

ARTICLE INFO

Article history:
Received 27 February 2013
Accepted 23 May 2013

Keywords:
Leaf area index
PROSAIL
Hyperspectral
Look-up table
Dual-angle observations

ABSTRACT

Leaf area index (LAI) is a key variable for modeling energy and mass exchange between the land surface and the atmosphere. Inversion of physically based radiative transfer models is the most established technique for estimating LAI from remotely sensed data. This study aims to evaluate the suitability of the PROSAIL model for LAI estimation of three typical row crops (maize, potato, and sunflower) from unmanned aerial vehicle (UAV) hyperspectral data. LAI was estimated using a look-up table (LUT) based on the inversion of the PROSAIL model. The estimated LAI was evaluated against *in situ* LAI measurements. The results indicated that the LUT-based inversion of the PROSAIL model was suitable for LAI estimation of these three crops, with a root mean square error (RMSE) of approximately 0.62 m^2 m^{-2}, and a relative RMSE (RRMSE) of approximately 15.5%. Dual-angle observations were also used to estimate LAI and proved to be more accurate than single-angle observations, with an RMSE of approximately 0.55 m^2 m^{-2} and an RRMSE of approximately 13.6%. The results demonstrate that additional directional information improves the performance of LAI estimation.

1. Introduction

Leaf area index (LAI), defined as the total one-sided area of leaves per unit of ground area (Bréda, 2003), is a key parameter in a wide range of biological and physical processes (Gower et al., 1999; Li et al., 2009; Myneni et al., 2002). For instance, the monitoring and mapping of LAI is vital for modeling energy and mass exchange between the land surface and the atmosphere (Asner et al., 2003; Running et al., 1999; Li et al., 2009). Remote sensing provides a cost-effective method to estimate LAI over extended regions. There are two main approaches for estimating LAI from remotely sensed data: statistical and physical approaches (Baret and Buis, 2008; Dorigo et al., 2007; Kimes et al., 2000). The statistical approaches are based on empirical relationships between ground-based LAI measurements and spectral vegetation indices (Darvishzadeh et al., 2008a; Haboudane et al., 2004). The physical approaches are based on radiative transfer model (RTM) inversion (Combal et al., 2002a; Meroni et al., 2004). The inversion of RTMs has been integrated multi-angular sensors (Dorigo, 2012; Meroni et al., 2004; Vuolo et al., 2008).

Three different techniques are commonly used for the inversion of RTMs: iterative optimization techniques (Jacquemoud et al., 1995; Meroni et al., 2004; Vohland et al., 2010), look-up tables (LUTs) (Darvishzadeh et al., 2012; Dorigo, 2012; Richter et al., 2011), and neural networks (NNs) (Atzberger, 2004; Bacour et al., 2006; Baret et al., 2007). Several studies have found that LUTs and NNs delivered the best accuracy and speed in the inversion of RTMs (Richter et al., 2009; Weiss et al., 2000). The inversion of RTMs is, by nature, an ill-posed problem for two main reasons (Atzberger, 2004; Combal et al., 2002a). One reason is that various combinations of canopy biophysical variables may produce similar canopy reflectance spectra. The other is that measurement and model uncertainties may induce large inaccuracy in the simulated reflectance spectra.

* Corresponding author at: Key Laboratory of Agri-informatics, Ministry of Agriculture/Institute of Agricultural Resources and Regional Planning, Chinese Academy of Agricultural Sciences, Beijing 100081, China. Tel.: +86 1082105077.
E-mail addresses: lizhaoliang@caas.cn, lizl@unistra.fr (Z.-L. Li).

0303-2434/$ – see front matter © 2013 Elsevier B.V. All rights reserved.
http://dx.doi.org/10.1016/j.jag.2013.05.007

Different strategies have been proposed to solve the ill-posed inverse problem (Li et al., 2013a, 2013b). For LUT-based inversion methods, the use of multiple solutions (rather than the single best solution) modestly increases the robustness of LAI estimation (Darvishzadeh et al., 2011; Weiss et al., 2000). The exploitation of *a priori* knowledge, *e.g.*, on the ranges and distributions of variables (Darvishzadeh et al., 2008b; Si et al., 2012) and on land cover classification (Dorigo et al., 2009; Verrelst et al., 2012), is another way to constrain solutions to the ill-posed problem and to improve the accuracy of LAI estimation. Moreover, the use of multi-angle observations has also been shown to improve the accuracy of LAI estimation (Dorigo, 2012; Meroni et al., 2004; Vuolo et al., 2008).

Because of its ease of use and general robustness, the PROSAIL model has been used to estimate LAI over fields of agricultural crops such as sugar beet (Combal et al., 2002b; Jacquemoud et al., 1995), maize (Koetz et al., 2005; Yang et al., 2012), and alfalfa (Bacour et al., 2002; Vuolo et al., 2008). However, relatively few investigations have been performed over potato and sunflower fields. The objective of this study is twofold: (i) to further evaluate the suitability of the PROSAIL model for LAI estimation of maize, potato, and sunflower fields in northern China using the LUT approach; and (ii) to compare the performance of LAI estimation from single- and dual-angle observations against *in situ* measurements. This paper is organized as follows. The study area, data, and methods are described in Section 2. The results are presented in Section 3 and discussed in Section 4. Conclusions are drawn in the last section.

2. Materials and methods

2.1. Study area

To evaluate a potential calibration and validation test field for future hyperspectral sensors, a comprehensive field campaign was conducted over the Baotou test site (Inner Mongolia, China, 40.88° N, 109.53° E) on 3 September 2011. The Baotou test site has an average ground elevation of approximately 1.3 km above sea level. The test site receives little precipitation and has a high percentage of cloud-free days. This area has a continental climate that is characterized by four seasons and a large diurnal temperature variation. The yearly average temperature is 6–7 °C, and the average annual rainfall is 200–250 mm. The main agricultural crops of this region are maize, potato, and sunflower, and all three require irrigation.

2.2. Data

2.2.1. In situ measurements

Four reference targets, which were 15 m × 15 m and with nominal reflectance of 20%, 30%, 40%, and 50%, were placed on a soil background over the study area. These four targets were used to perform the radiometric calibration of unmanned aerial vehicle (UAV) hyperspectral sensor. *In situ* surface reflectance spectra of these four targets were collected with an SVC HR-1024 field-portable spectroradiometer at the time of UAV hyperspectral data acquisition. The spectroradiometer has 1024 channels covering the spectral range from 350 to 2500 nm with spectral resolution of 3.5 nm at 700 nm wavelength, 9.5 nm at 1500 nm wavelength, and 6.5 nm at 2100 nm wavelength. Before and after each target measurement, a reference measurement was collected with a white Spectralon reference panel. The spectra were measured in absolute radiance mode at nadir. The raw spectra of each target were scaled with the reference measurements to produce reflectance spectra. Five measurements of each target were averaged to yield a representative reflectance spectrum.

Atmospheric measurements were collected with an automatic CIMEL CE318 sunphotometer at the time of the UAV hyperspectral data acquisition. The sunphotometer has nine channels at nominal wavelengths of 340, 380, 440, 500, 670, 870, 936, 1020, and 1640 nm. Measurements at 936 nm were used to derive columnar water vapor (CWV) (Bruegge et al., 1992) with the coefficients simulated by MODTRAN (Halthore et al., 1997). Aerosol optical depth (AOD) at 550 nm was derived from the other channels using the Ångström law, following the method of Estellés et al. (2006). The measured values of AOD at 550 nm and CWV at the time of UAV hyperspectral data acquisition were 0.18 and 1.7 g cm^{-2}, respectively. These values were used as inputs to atmospheric radiative transfer models such as MODTRAN to perform atmospheric corrections on the UAV hyperspectral data.

In situ LAI measurements were collected with the Plant Canopy Analyzer LAI-2200 instrument under overcast sky conditions on 2 September 2011. The average LAI was calculated in each sample plot based on the one above-canopy measurement and five below-canopy measurements. When LAI measurements were conducted, the sun was kept behind the operator and the operator used a view restrictor of 45°. No corrections were performed to account for leaf clumping or the influence of non-photosynthetic plant components (*e.g.*, stems). A total of 14 LAI measurements were performed: 4 on maize, 4 on potato, and 6 on sunflower plots. The measured LAI values ranged from 2.4 to 3.2 m^2 m^{-2} for maize, 4.0–4.8 m^2 m^{-2} for potato, and 1.9–4.8 m^2 m^{-2} for sunflower. The *in situ* LAI measurements were used to evaluate the accuracy of LAI estimation from hyperspectral data.

2.2.2. UAV hyperspectral data

Two flight lines were acquired by a new hyperspectral sensor over the study area on 3 September 2011 from approximately 14:40 to 15:00 local time. This hyperspectral sensor is referred to as UAV-HYPER and was installed on a UAV. The UAV-HYPER sensor contains 128 bands that cover the spectral range from 350 to 1030 nm, with a bandwidth of 5 nm and a field of view of 11.5°. During the campaign, the operational altitude of the UAV-HYPER sensor was approximately 3.5 km above ground level, which gave a spatial resolution of approximately 0.7 m.

The two flight lines L1 (west–east) and L2 (east–west) overlap. The observation details of these two flight lines are summarized in Table 1, and subset images of the two flight lines are shown in Fig. 1. There are 10 sample plots located along flight line L1, 11 along flight line L2, and 7 in the overlapping area.

Pre-processing of the UAV-HYPER data includes the assessment of the signal-to-noise ratio (SNR), radiometric calibration, and atmospheric and geometric corrections. Some bands of the UAV-HYPER sensor have low SNR values. A method based on local means and local standard deviations of small imaging blocks was used to estimate SNR from the UAV-HYPER data (Gao, 1993). To minimize the effect of low SNR on the LAI retrieval, 32 bands with SNR values lower than 40 were discarded from further analysis: bands 1–12 (395.3–450.0 nm) and bands 109–128 (932.5–1027.0 nm). The radiometric calibration coefficients were determined using the four reference targets. The atmospheric correction was performed using a MODTRAN-based LUT method informed by atmospheric parameters collected at the time of the UAV-HYPER data acquisitions (Duan et al., 2013). The geometric correction was performed using differential GPS-derived ground control points. A second-order polynomial transformation with nearest-neighbor interpolation was used for the geometric correction, which achieved a geometric accuracy of approximately one pixel.

2.3. Method

2.3.1. Generation of the LUT

The PROSAIL model (Jacquemoud et al., 2009), which couples the PROSPECT leaf optical properties model (Jacquemoud and

Table 1
Acquisition time and sun-sensor geometry of the flight lines L1 and L2.

Flight line	Local time	SZA	SAA	VZA[a]			VAA	Orientation
				Min	Max	Mean		
L1	14:43	42.8°	227.5°	0.2°	4.7°	1.9°	172.2°	West–east
L2	14:53	44.2°	230.5°	0.9°	5.4°	3°	6.9°	East–west

SZA: solar zenith angle, SAA: solar azimuth angle, VZA: view zenith angle, and VAA: view azimuth angle.
[a] Minimum, maximum, and mean VZA values of sample plots in the flight lines L1 and L2.

Baret, 1990) with the SAIL canopy reflectance model (Verhoef, 1984, 1985), was selected to construct an LUT. This model has been widely validated and applied to reflectance modeling studies (Darvishzadeh et al., 2008b; Si et al., 2012).

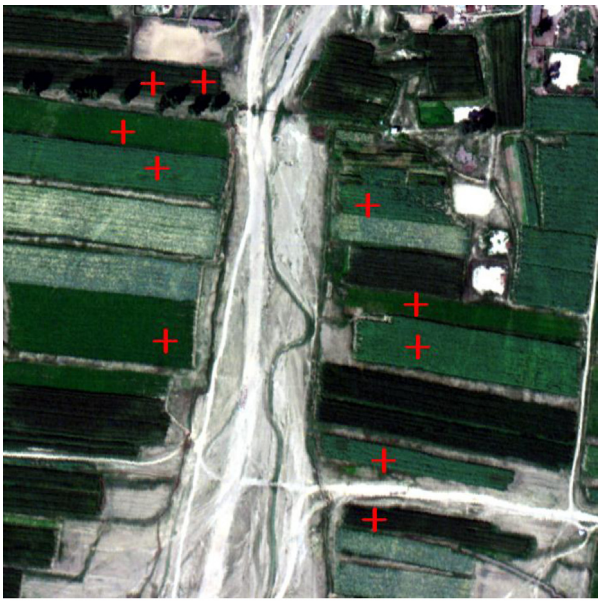

(a) Flight line L1

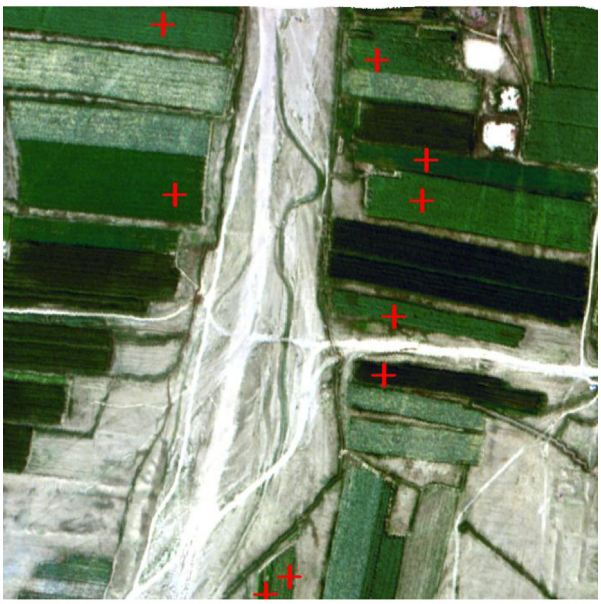

(b) Flight line L2

Fig. 1. Subset images of the flight lines (a) L1 (west–east) and (b) L2 (east–west) acquired over the study area. Plus signs denote LAI sample plots. Two additional LAI sample plots (not shown) exist outside the subset of the L2 image.

The PROSPECT model simulates the leaf hemispherical transmittance and reflectance as a function of four structural and biochemical leaf parameters: leaf structure parameter N (unitless), leaf chlorophyll $a+b$ concentration C_{ab} ($\mu g\,cm^{-2}$), equivalent water thickness C_w ($g\,cm^{-2}$), and dry matter content C_m ($g\,cm^{-2}$). The leaf optical properties (leaf reflectance and transmittance) simulated by the PROSPECT model are then inputted into the SAIL model. The SAIL model simulates the top-of-the-canopy reflectance as a function of eight input parameters: LAI ($m^2\,m^{-2}$), average leaf angle *ALA* (deg) of an ellipsoidal leaf angle distribution function (Campbell, 1990), fraction of diffuse incoming solar radiation *skyl* (unitless), wavelength-dependent canopy background reflectance (*i.e.*, soil reflectance), hot-spot size parameter *hot* ($m\,m^{-1}$) (Kuusk, 1995), sun zenith angle t_s (deg), sensor viewing angle t_o (deg), and relative azimuth angle *phi* (deg) between the sensor and sun.

To account for the variations in soil brightness induced by soil moisture and surface roughness, a soil brightness parameter (*scale*) was used to scale and shape an average soil spectrum (Darvishzadeh et al., 2012):

$$R_s = \text{scale} \times r_s \quad (1)$$

where r_s and R_s are the average soil spectrum before and after scaling, respectively.

To generate the LUT, the PROSAIL model was run in forward mode to simulate canopy reflectance for an appropriate number of parameter combinations. An LUT size of 100,000 parameter combinations was found to achieve a good compromise between the computer resource requirement and the accuracy of canopy variable estimation (Weiss et al., 2000). The same LUT was used for the LAI estimation of all three crops. The 100,000 parameter combinations were randomly generated with uniform distributions and specific ranges for the variables in Table 2:

$$V(n) = \min + (\max - \min) \times rand(n) \quad (2)$$

where V is the variable, n is the number of parameter combinations, *rand* is the uniform random number generator, and *min* and *max* are the minimum and maximum of the variable, respectively.

The ranges (minimum and maximum) of the variables (Table 2) were selected in accordance with previous studies (Darvishzadeh et al., 2011; Koetz et al., 2005; Richter et al., 2011; Si et al., 2012). The parameter *skyl* depends on atmospheric conditions, the solar zenith angle, and wavelength. Because it has only a very small influence on canopy reflectance, *skyl* was fixed at 0.1 across all

Table 2
Ranges of the input variables for the PROSAIL model for the generation of the LUT.

Variable	Abbr.	Unit	Minimum	Maximum
Leaf structure parameter	N	Unitless	1	2
Leaf chlorophyll concentration	C_{ab}	$\mu g\,cm^{-2}$	20	70
Dry matter content	C_m	$g\,cm^{-2}$	0.004	0.007
Equivalent water thickness	C_w	$g\,cm^{-2}$	0.005	0.03
Leaf area index	LAI	$m^2\,m^{-2}$	0.001	6
Average leaf angle	ALA	Deg	30	70
Hot-spot size parameter	*hot*	$m\,m^{-1}$	0.05	1
Soil brightness parameter	*scale*	Unitless	0.5	1.5

Table 3
Accuracy of LAI estimation from single-angle observations L1 and L2 for maize, potato, sunflower, and all crops. RRMSE is the RMSE divided by the average of the *in situ* LAI measurements.

Crop type	L1		L2	
	RMSE ($m^2\ m^{-2}$)	RRMSE (%)	RMSE ($m^2\ m^{-2}$)	RRMSE (%)
Maize	0.58	21.1	0.96	31.1
Potato	0.62	14.2	0.22	5.2
Sunflower	0.45	10.6	0.39	10.3
All crops	0.55	14.3	0.51	13.6

wavelengths, as in previous studies (Atzberger and Richter, 2012; Darvishzadeh et al., 2008b; Richter et al., 2009; Vuolo et al., 2008). A soil reflectance spectrum corresponding to an average of local measurements was used to characterize the background reflectance. Sun-sensor geometry corresponding to the situation of the UAV-HYPER data acquisitions (see Table 1).

2.3.2. Inversion of the LUT

To select the solution of the inverse problem, the LUT is sorted in terms of the cost function χ_{RMSE} corresponding to the RMSE between the measured reflectance $R_{measured}$ and the simulated reflectance $R_{simulated}$ found in the LUT (Combal et al., 2002a; Vohland et al., 2010):

$$\chi_{RMSE} = \sqrt{\frac{1}{n_d \cdot n_b}\sum_{i=1}^{n_d}\sum_{j=1}^{n_b}\left(R^{i,j}_{measured} - R^{i,j}_{simulated}\right)^2} \quad (3)$$

where n_d is the number of viewing directions and n_b is the number of bands.

The solution is found by identifying the set of variables in the LUT that minimize the χ_{RMSE} value. However, because measurement errors and model inadequacies make this an ill-posed problem, the solution may not be unique. For this reason, the solution is the average of the parameter combinations that yield within 20% of the smallest χ_{RMSE} value. The 20% threshold is consistent with the optimum number adopted by previous studies (*e.g.*, Dorigo, 2012; Koetz et al., 2005; Vohland et al., 2010).

3. Results

3.1. LAI estimation from single-angle observations

The LUT-based inversion of the PROSAIL model was performed to estimate LAI from the single-angle observations (SAOs) L1 and L2. The LAI was averaged over 3 × 3 pixel windows centered at each sample plot. The estimated LAIs from the SAOs L1 and L2 *versus* the *in situ* LAI measurements are shown in Fig. 2(a) and (b), respectively, and are summarized in Table 3. Horizontal error bars denote ±1 standard deviation of the *in situ* LAI measurements at each sample plot. Vertical error bars indicate ±1 standard deviation of the estimated LAI in the 3 × 3 pixel windows centered at each sample plot. The accuracy of the LAI estimation was evaluated in terms of the RMSE and relative RMSE, where RRMSE is the RMSE divided by the average of the *in situ* LAI measurements.

As displayed in Fig. 2, the estimated LAI from the SAO L1 slightly overestimated the *in situ* LAI measurements for some sample plots where LAI values exceeded 3.5, with RMSE of 0.55 $m^2\ m^{-2}$ and RRMSE of 14.3%, whereas the estimated LAI from the SAO L2 slightly underestimated the *in situ* LAI measurements for some sample plots, with RMSE of 0.51 $m^2\ m^{-2}$ and RRMSE of 13.6%. Table 3 shows the accuracy of the LAI estimation from the SAOs L1 and L2 for maize, potato, sunflower, and all crops. For the SAO L1, the RMSE value decreases from 0.62 $m^2\ m^{-2}$ for potato and 0.58 $m^2\ m^{-2}$ for maize to 0.45 $m^2\ m^{-2}$ for sunflower, whereas the

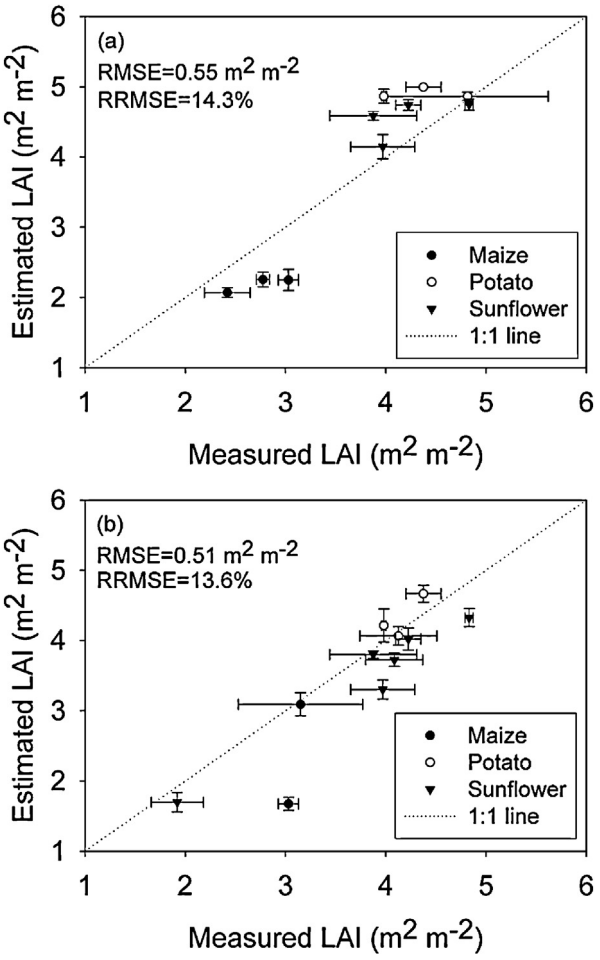

Fig. 2. Comparison between the *in situ* LAI measurements and the estimated LAI from single-angle observations (a) L1 and (b) L2, respectively. Horizontal error bars denote ±1 standard deviation of the *in situ* LAI measurements at each sample plot. Vertical error bars indicate ±1 standard deviation of the estimated LAI in 3 × 3 pixel windows centered on each sample plot. RRMSE is the RMSE divided by the average of the *in situ* LAI measurements.

RRMSE value decreases from 21.1% for maize and 14.2% for potato to 10.6% for sunflower. For the SAO L2, the RMSE value decreases from 0.96 $m^2\ m^{-2}$ for maize and 0.39 $m^2\ m^{-2}$ for sunflower to 0.22 $m^2\ m^{-2}$ for potato, whereas the RRMSE value decreases from 31.1% for maize and 10.3% for sunflower to 5.2% for potato. Nevertheless, the accuracy of LAI estimation for all crops is similar for the SAOs L1 and L2.

3.2. LAI estimation from dual-angle observations

The two overlapping flight lines L1 and L2 provide an opportunity to estimate LAI from dual-angle observations (DAOs). Prior to applying the model inversion to estimate LAI from the DAO, it is necessary to evaluate whether the LAI estimation from the SAOs L1 and L2 is robust. Fig. 3 shows the estimated LAI from the SAO L1 *versus* the estimated LAI from the SAO L2 for 7 sample plots in the overlapping area of the two flight lines. There are discrepancies between the LAI estimated from the SAOs L1 and L2: the estimated LAI from the SAO L1 is higher than that from the SAO L2 for the 7 sample plots. These results indicate that integrating the SAOs L1 and L2 simultaneously into the inversion scheme may improve the accuracy of LAI estimation.

To further check whether including a second observation angle adds the angular anisotropy information, anisotropy index *versus* wavelength for the 7 sample plots is shown in Fig. 4. The specific

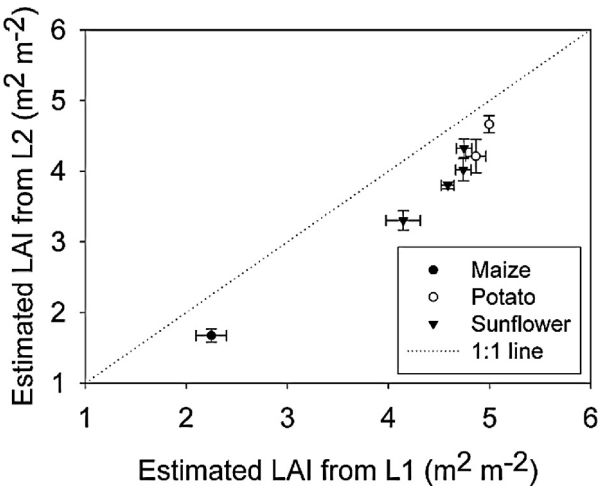

Fig. 3. Comparison between the estimated LAI from single-angle observations L1 and L2. Horizontal error bars denote ±1 standard deviation of the estimated LAI from L1 at each sample plot. Vertical error bars indicate ±1 standard deviation of the estimated LAI from L2 at each sample plot.

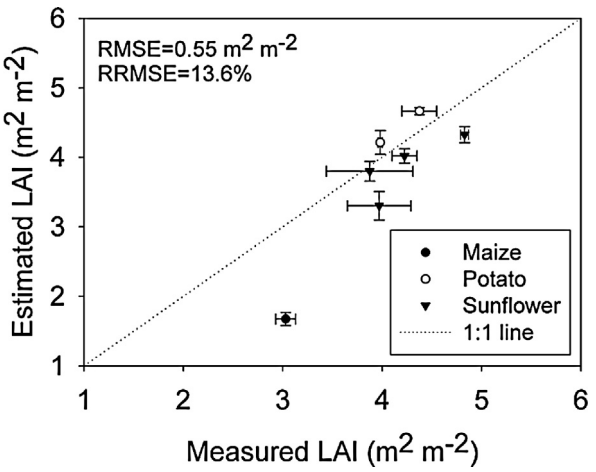

Fig. 5. Comparison between the *in situ* LAI measurements and the estimated LAI from dual-angle observations. Horizontal error bars denote ±1 standard deviation of the *in situ* LAI measurements at each sample plot. Vertical error bars indicate ±1 standard deviation of the estimated LAI in 3 × 3 pixel windows centered on each sample plot. RRMSE is the RMSE divided by the average of the *in situ* LAI measurements.

definition of the anisotropy index can be found in Sandmeier et al. (1998). In our study, the anisotropy index is calculated as the ratio of surface reflectance of the SAOs L1 and L2 for each of the 7 sample plots. As the surface reflectance of these 7 samples plots retrieved from SAOs L1 and L2 below approximately 0.52 μm is very small (<0.05), their ratio may lead to high (>4.0) or low (<1.0) anisotropy index values. Considering the uncertainties involved in the surface reflectance retrieval, the anisotropy index below approximately 0.52 μm should be taken with caution here. As seen from Fig. 4, the values of the anisotropy index range from approximately 1.2 to 2.0 in the wavelength range between approximately 0.52 and 0.7 μm. There are relative strong anisotropy effects around 0.7 μm (red region) and relative low anisotropy effects around 0.56 μm (green region) for some sample plots due to the strong chlorophyll absorbance in red region and low in green region (Sandmeier et al., 1998). The values of the anisotropy index are lower than approximately 1.2 in the spectral region above approximately 0.7 μm due to the multiple scattering effects which reduce the contrast between shadowed and illuminated canopy components and result in small anisotropy effects (Dorigo, 2012).

The accuracy of LAI estimation from the DAO for all crops is shown in Fig. 5. Horizontal error bars are ±1 standard deviation of the *in situ* LAI measurements at each sample plot. Vertical error bars represent ±1 standard deviation of the estimated LAI in 3 × 3 pixel windows centered at each sample plot. A comparison of the accuracy of LAI estimation between the SAO and the DAO was performed in the overlapping area of the flight lines. There are 7 sample plots in this area, with the measured LAI values ranging from 3.0 to 4.8 $m^2\ m^{-2}$. The accuracy of LAI estimation from the DAO was evaluated using these 7 sample plots. In addition, the accuracy of LAI estimation from the SAOs L1 and L2 was also re-calculated using these 7 sample plots. These results are shown in Table 4. The accuracy of LAI estimation from the DAO is slightly higher than that from the SAOs L1 and L2. The RMSE value decreases from 0.61 $m^2\ m^{-2}$ for the SAO L1 and 0.62 $m^2\ m^{-2}$ for the SAO L2 to 0.55 $m^2\ m^{-2}$ for the DAO. Moreover, the RRMSE value decreases from 15.1% for the SAO L1 and 15.5% for the SAO L2 to 13.6% for the DAO.

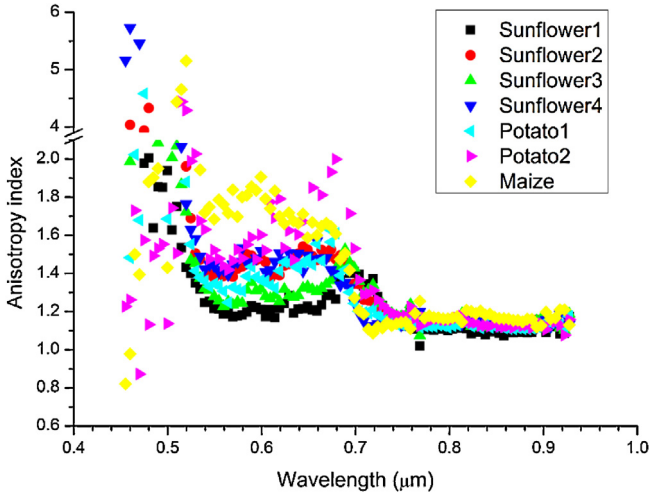

Fig. 4. Anisotropy index *versus* wavelength for the 7 sample plots in the overlapping area of the flight lines L1 and L2.

3.3. Comparison between different LUT sizes

To analyze the influence of different LUT sizes on the accuracy of LAI estimation, two more LUTs with sizes of 50,000 and 250,000 were generated using the same uniform distributions and ranges of the variables as the LUT with a size of 100,000. The LAI estimation was performed for the SAO and the DAO using different LUT sizes. The results are shown in Table 5. There is no significant difference between the accuracy of LAI estimation using different LUT sizes. Similar results were obtained by Darvishzadeh et al. (2012), who used three different LUT sizes (50,000, 100,000, and 250,000) to estimate canopy chlorophyll content. They concluded that the size of the LUT was not significantly important for canopy chlorophyll content retrieval when the inverse problem had more than 100 viable solutions. In addition, Richter et al. (2009) compared two LUTs with sizes of 100,000 and 200,000 for LAI estimation and found that the larger LUT did not improve the accuracy of the LAI

Table 4
Accuracy of LAI estimation from single-angle observations (SAOs) and dual-angle observations (DAOs). RRMSE is the RMSE divided by the average of the *in situ* LAI measurements.

Data	RMSE ($m^2\ m^{-2}$)	RRMSE (%)
SAO L1	0.61	15.1
SAO L2	0.62	15.5
DAO	0.55	13.6

Table 5
Accuracy of LAI estimation from single-angle observations (SAOs) and dual-angle observations (DAOs) using different LUT sizes. RRMSE is the RMSE divided by the average of the *in situ* LAI measurements.

Data	50,000		100,000		250,000	
	RMSE ($m^2\ m^{-2}$)	RRMSE (%)	RMSE ($m^2\ m^{-2}$)	RRMSE (%)	RMSE ($m^2\ m^{-2}$)	RRMSE (%)
SAO L1	0.60	14.9	0.61	15.1	0.61	15.0
SAO L2	0.63	15.5	0.62	15.5	0.63	15.5
DAO	0.55	13.6	0.55	13.6	0.55	13.7

estimation. Therefore, following Weiss et al. (2000), this study uses an LUT size of 100,000 – a good compromise between accuracy and computer resources – to estimate the LAI from the SAO and the DAO.

3.4. Comparison of different cost functions

To assess the influence of different cost functions on the accuracy of LAI estimation, a second cost function was also used in the model inversion. This cost function, χ_{RRMSE}, corresponds to the RRMSE between the measured reflectance $R_{measured}$ and the simulated reflectance $R_{simulated}$ found in the LUT (Weiss et al., 2000):

$$\chi_{RRMSE} = \sqrt{\frac{1}{n_d \cdot n_b}\sum_{i=1}^{n_d}\sum_{j=1}^{n_b}\left(\frac{R^{i,j}_{measured} - R^{i,j}_{simulated}}{R^{i,j}_{measured}}\right)^2} \quad (4)$$

Fig. 6(a) and (b) show the *in situ* LAI measurements *versus* the estimated LAI from the SAOs L1 and L2 using the cost function χ_{RRMSE}. The RMSE and RRMSE values are 0.82 $m^2\ m^{-2}$ and 21.3% for the SAO L1, and 0.60 $m^2\ m^{-2}$ and 16.0% for the SAO L2. As the difference between Fig. 6(a) and (b) and Fig. 2(a) and (b) shows, the LAI estimation using the cost function χ_{RRMSE} is less accurate than that using the cost function χ_{RMSE}. As the difference between Fig. 6(c) and Fig. 5 shows, similar results are achieved for the DAO: the RMSE and RRMSE values are 0.66 $m^2\ m^{-2}$ and 16.4% for the cost function χ_{RRMSE}, and 0.55 $m^2\ m^{-2}$ and 13.6% for the cost function χ_{RMSE}. Because of its better accuracy, we used the cost function χ_{RMSE} more often in this study.

4. Discussion

4.1. Impact of row crops on the model inversion

Fig. 2 indicates that the estimated LAI from the SAO L1 was often slightly greater than the measured LAI for LAI values above 3.5, whereas the estimated LAI from the SAO L2 was often slightly less than the measured LAI. These results may be because the PROSAIL model does not take into account the shading effect of row crops (Dorigo, 2012). The shading effect results in enhanced reflectance in the backward scattering direction (the perspective of SAO L1) and in reduced reflectance in the forward scattering direction (the perspective of SAO L2), as observed in Fig. 7. Similar results were obtained by Schlerf and Atzberger (2012) and Verrelst et al. (2012), who used the multi-angular CHRIS/PROBA data to estimate LAI.

The results shown in Fig. 2 also demonstrate a significant underestimation in the estimated LAI for maize. This may be because the PROSAIL model was initially developed for canopies for which the turbid medium assumption, where the leaves are randomly distributed within the canopy volume (Jacquemoud et al., 2009), is valid. The canopy characteristics of maize deviate from this assumption. Maize, a typical row crop, is affected by leaf clumping, which the PROSAIL model does not take into account. Therefore, the PROSAIL model underestimated maize LAI compared to the *in situ* LAI measurements. Similar results were described in other studies (*e.g.*, Richter et al., 2009, 2011). To reduce the effect of

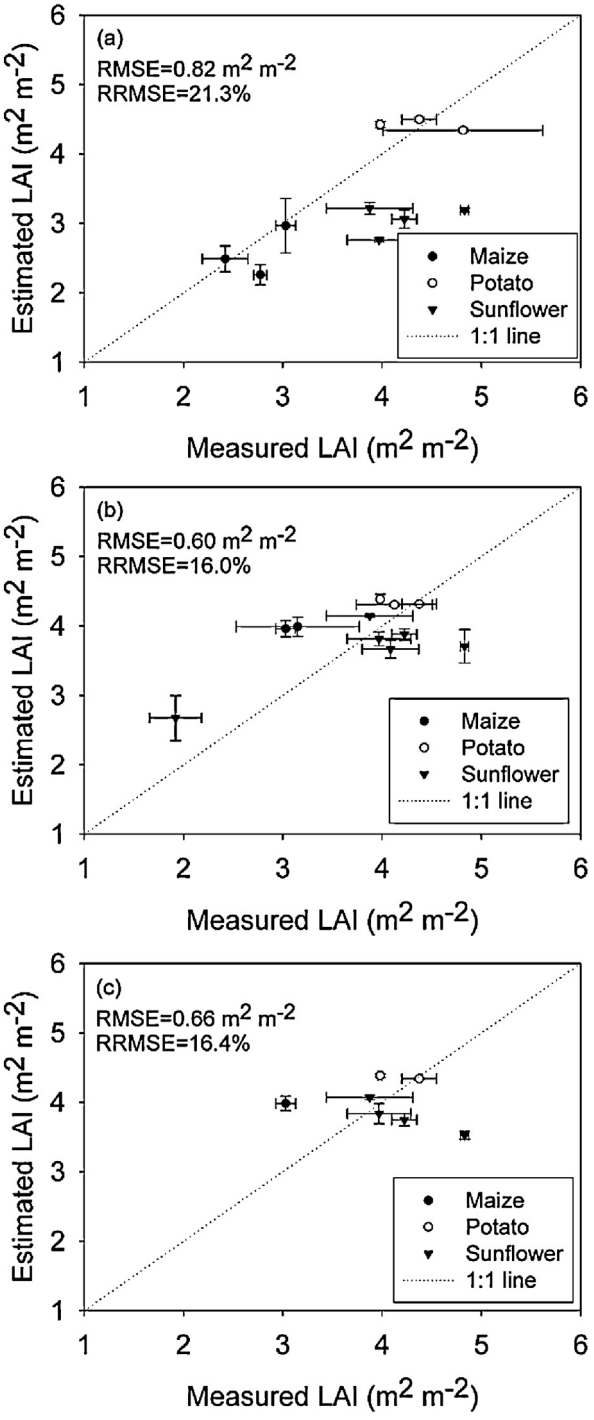

Fig. 6. Comparison between the *in situ* LAI measurements and the estimated LAI from single-angle observations (a) L1 and (b) L2 and (c) dual-angle observations using the cost function χ_{RRMSE} (Eq. (4)). RRMSE is the RMSE divided by the average of the *in situ* LAI measurements.

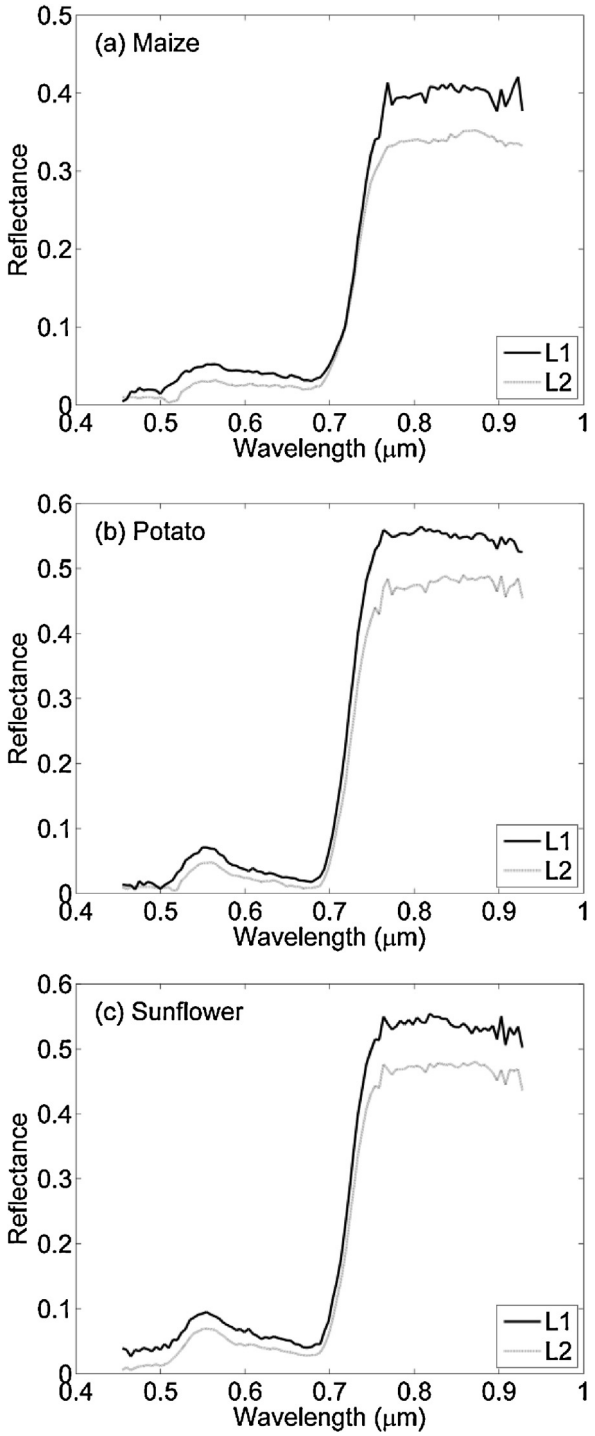

Fig. 7. Measured surface reflectance from single-angle observations L1 and L2 for (a) maize, (b) potato, and (c) sunflower.

row structure on the estimation of LAI for maize, Yao et al. (2008) proposed to use a row structure model for early growth stage (before elongation) and a homogeneous canopy model for later growth stage (after elongation).

LAI estimation for potato and sunflower yielded lower RRMSE values than for maize. This result may be because potato and sunflower fields exhibited more homogeneous coverage than maize fields. Except for one sunflower sample plot, the measured LAI values for potato and sunflower are higher than 4 m^2 m^{-2}, whereas those for maize are lower than 3.5 m^2 m^{-2}. Consequently, the soil background has a smaller influence on the LAI estimation for potato and sunflower fields than for maize fields.

Improving the accuracy of LAI estimation for row crops requires hybrid turbid/geometrical models that take row structure into account. For example, coupling the improved PROSPECT model (Feret et al., 2008) with a canopy reflectance model accounting for row structure (*e.g.*, Zhao et al., 2010) will improve the accuracy of LAI estimation. Nevertheless, the inversion of such a model requires high parameterization loads, which come at the expense of conceptual and computational complexity.

4.2. Impact of the ill-posed inverse problem

The LUT-based inversion of the PROSAIL model is, by nature, an ill-posed problem because various combinations of canopy parameters may yield similar spectra. Combal et al. (2002a) showed that the use of *a priori* information is an efficient way to solve the ill-posed problem and to improve the accuracy of LAI estimation. Later studies used *a priori* information on the distributions and ranges of the variables to regularize the ill-posed inverse problem (Darvishzadeh et al., 2008b; Si et al., 2012). In this study, we use the approximate ranges from the *in situ* measurements of the parameters LAI and ALA as *a priori* information to generate the LUT. The sun zenith angle, the sensor viewing angle, and the relative azimuth angle were fixed at the sun-sensor geometry of the UAV-HYPER data acquisitions, but the other input parameters were constrained *a priori* to ranges defined by the results of previous studies.

Due to the lack of *a priori* information on variables for each separate crop species, we generated the same LUT for maize, potato, and sunflower. However, the differences in the accuracy of LAI estimation demonstrate that the use of a well-adapted parameter input set for each crop species may improve the accuracy of LAI estimation. To constrain the ranges of variables, Dorigo et al. (2009) and Verrelst et al. (2012) used land cover classification to construct a specific LUT for each vegetation class.

Selecting the cost function of the model inversion is a critical step in solving the ill-posed inverse problem. Meroni et al. (2004) showed that better accuracy was achieved using a cost function that included radiometric and priori information than using a cost function that included only radiometric information. However, often, only limited information about the crop status in an agricultural area is available, so the cost functions in this study were often constrained by radiometric information only. We compared two cost functions χ_{RMSE} (Eq. (3)) and χ_{RRMSE} (Eq. (4)). The accuracy of LAI estimation using the cost function χ_{RMSE} was higher than that using the cost function χ_{RRMSE}.

The use of multi-angle observations instead of just the nadir view has also proven to be an efficient way to constrain the ill-posed problem. This aspect is discussed in the following section.

4.3. Multi-angle observations

Table 5 shows that the DAO gave a more accurate LAI estimation than did the SAO. The results are consistent with those obtained by Dorigo (2012), Meroni et al. (2004), Vuolo et al. (2008), and Yang et al. (2011), who showed that directional information improves the accuracy of LAI estimation. There were only two angle observations available for each pixel in this study, and their angular anisotropy differed by only small amounts. Consequently, the RMSE (RRMSE) value of the LAI estimation from the DAO was only approximately 0.05 m^2 m^{-2} (2%) lower than that from the SAO. If more angle observations can be acquired for each pixel, the accuracy of LAI estimation may be further improved. However, more angle observations may also add to the uncertainty of the LAI estimation. For example, Dorigo (2012) showed that including the +55° viewing angle of the CHRIS/PROBA in the inversion scheme dramatically reduced the

accuracy of LAI estimation. Therefore, optimal directional sampling is necessary to obtain high accuracy of LAI estimation.

5. Conclusions

This study investigated the performance of LUT-based inversion of the PROSAIL model for LAI estimation from the UAV-HYPER data. LAI estimation was performed along two overlapping flight lines, L1 and L2, in a study area over three typical row crops: maize, potato, and sunflower. *In situ* LAI measurements were also collected. The estimated LAI was evaluated against the *in situ* LAI measurements in terms of the RMSE and RRMSE. For the SAO L1, the best-performing crop was sunflower, with an RMSE of 0.45 m^2 m^{-2} and an RRMSE of 10.6%, and the worst-performing crop was potato, with an RMSE of 0.62 m^2 m^{-2} and an RRMSE of 14.2%. For the SAO L2, the best accuracy was achieved for potato, with an RMSE of 0.22 m^2 m^{-2} and an RRMSE of 5.2%, whereas the worst accuracy was achieved for maize, with an RMSE of 0.96 m^2 m^{-2} and an RRMSE of 31.1%. Nevertheless, the accuracy of LAI estimation for all crops was similar for the SAOs L1 and L2. These results indicate that the PROSAIL model is suitable for LAI estimation for these three crops with reasonable accuracy in terms of the RMSE and RRMSE.

The UAV-HYPER data in the area where the flight lines overlapped provided an opportunity to estimate LAI from the DAO. The estimated LAI from the SAO and the DAO were compared against the *in situ* LAI measurements. The RMSE (RRMSE) value was approximately 0.62 m^2 m^{-2} (15.5%) for the SAO and approximately 0.55 m^2 m^{-2} (13.6%) for the DAO. These results show that using the DAO rather than the SAO improves the accuracy of LAI. The effects of different LUT sizes on the accuracy of LAI estimation were also investigated. The results demonstrate that the size of the LUT does not affect the accuracy of the LAI estimation. The impact of different cost functions on the accuracy of LAI estimation was also analyzed. The results showed that the choice of cost function influences the accuracy of LAI estimation.

Acknowledgements

This work was supported by the Hi-Tech Research and Development Program of China (863 Plan Program) under Grant 2012AA12A302 and by the State Key Laboratory of Resources and Environment Information System under Grant 088RA801KA. Mr. Si-Bo Duan is financially supported by the China Scholarship Council for his stay in ICube, France.

References

Asner, G.P., Scurlock, J.M.O., Hicke, J.A., 2003. Global synthesis of leaf area index observations: implications for ecological and remote sensing studies. Global Ecology and Biogeography 12, 191–205.

Atzberger, C., 2004. Object-based retrieval of biophysical canopy variables using artificial neural nets and radiative transfer models. Remote Sensing of Environment 93, 53–67.

Atzberger, C., Richter, K., 2012. Spatially constrained inversion of radiative transfer models for improved LAI mapping from future Sentinel-2 imagery. Remote Sensing of Environment 120, 208–218.

Bacour, C., Baret, F., Béal, D., Weiss, M., Pavageau, K., 2006. Neural network estimation of LAI, fAPAR, fCover and LAI × Cab, from top of canopy MERIS reflectance data: principles and validation. Remote Sensing of Environment 105, 313–325.

Bacour, C., Jacquemoud, S., Leroy, M., Hautecœur, O., Weiss, M., Prévot, L., Bruguier, N., Chauki, H., 2002. Reliability of the estimation of vegetation characteristics by inversion of three canopy reflectance models on airborne POLDER data. Agronomie 22, 555–565.

Baret, F., Buis, S., 2008. Estimating canopy characteristics from remote sensing observations: review of methods and associated problems. In: Liang, S. (Ed.), Advances in Land Remote Sensing: System, Modeling, Inversion and Application. Springer, pp. 173–201.

Baret, F., Hagolle, O., Geiger, B., Bicheron, P., Miras, B., Huc, M., Berthelot, B., Niño, F., Weiss, M., Samain, O., Roujean, J.L., Leroy, M., 2007. LAI, fAPAR and fCover CYCLOPES global products derived from VEGETATION. Part 1: principles of the algorithm. Remote Sensing of Environment 110, 275–286.

Bréda, N.J.J., 2003. Ground-based measurements of leaf area index: a review of methods, instruments and current controversies. Journal of Experimental Botany 54, 2403–2417.

Bruegge, C.J., Conel, J.E., Green, R.O., Margolis, J.S., Holm, R.G., Toon, G., 1992. Water vapor column abundance retrievals during FIFE. Journal of Geophysical Research 97, 18759–18768.

Campbell, G.S., 1990. Derivation of an angle density function for canopies with ellipsoidal leaf angle distributions. Agricultural and Forest Meteorology 49, 173–176.

Combal, B., Baret, F., Weiss, M., Trubuil, A., Mace, D., Pragnere, A., Myneni, R., Knyazikhin, Y., Wang, L., 2002a. Retrieval of canopy biophysical variables from bidirectional reflectance-using prior information to solve the ill-posed inverse problem. *Remote Sensing of Environment* 84, 1–15.

Combal, B., Baret, F., Weiss, M., 2002b. Improving canopy variables estimation from remote sensing data by exploiting ancillary information. Case study on sugar beet canopies. Agronomie 22, 205–215.

Darvishzadeh, R., Skidmore, A., Atzberger, C., van Wieren, S., 2008a. Estimation of vegetation LAI from hyperspectral reflectance data: effects of soil type and plant architecture. International Journal of Applied Earth Observation and Geoinformation 10, 358–373.

Darvishzadeh, R., Atzberger, C., Skidmore, A., Schlerf, M., 2011. Mapping grassland leaf area index with airborne hyperspectral imagery: a comparison study of statistical approaches and inversion of radiative transfer models. ISPRS Journal of Photogrammetry and Remote Sensing 66, 894–906.

Darvishzadeh, R., Matkan, A.A., Ahangar, A.D., 2012. Inversion of a radiative transfer model for estimation of rice canopy chlorophyll content using a lookup-table approach. IEEE Journal of Selected Topics in Applied Earth Observations and Remote Sensing 5, 1222–1230.

Darvishzadeh, R., Skidmore, A., Schlerf, M., Atzberger, C., 2008b. Inversion of a radiative transfer model for estimating vegetation LAI and chlorophyll in a heterogeneous grassland. Remote Sensing of Environment 112, 2592–2604.

Dorigo, W.A., 2012. Improving the robustness of cotton status characterisation by radiative transfer model inversion of multi-angular CHRIS/PROBA data. IEEE Journal of Selected Topics in Applied Earth Observations and Remote Sensing 5, 18–29.

Dorigo, W., Richter, R., Baret, F., Bamler, R., Wagner, W., 2009. Enhanced automated canopy characterization from hyperspectral data by a novel two step radiative transfer model inversion approach. Remote Sensing 1, 1139–1170.

Dorigo, W.A., Zurita-Milla, R., de Wit, A.J.W., Brazile, J., Singh, R., Schaepman, M.E., 2007. A review on reflective remote sensing and data assimilation techniques for enhanced agroecosystem modeling. International Journal of Applied Earth Observation and Geoinformation 9, 165–193.

Duan, S.-B., Li, Z.-L., Tang, B.-H., Wu, H., Ma, L., Zhao, E., Li, C., 2013. Land surface reflectance retrieval from hyperspectral data collected by an unmanned aerial vehicle over the Baotou test site. PLoS ONE, http://dx.doi.org/10.1371/journal.pone.0066972.

Estellés, V., Utrillas, M.P., Martínez-Lozano, J.A., Alcántara, A., Alados-Arboledas, L., Olmo, F.J., Lorente, J., de Cabo, X., Cachorro, V., Horvath, H., Labajo, A., Sorribas, M., Díaz, J.P., Díaz, A.M., Silva, A.M., Elías, T., Pujadas, M., Rodrigues, J.A., Cañada, J., García, Y., 2006. Intercomparison of spectroradiometers and Sun photometers for the determination of the aerosol optical depth during the VELETA-2002 field campaign. Journal of Geophysical Research 111, D17207, http://dx.doi.org/10.1029/2005JD006047.

Feret, J.-B., François, C., Asner, G.P., Gitelson, A.A., Martin, R.E., Bidel, L.P.R., Ustin, S.L., le Maire, G., Jacquemoud, S., 2008. PROSPECT-4 and 5: advances in the leaf optical properties model separating photosynthetic pigments. Remote Sensing of Environment 112, 3030–3043.

Gao, B.-C., 1993. An operational method for estimating signal to noise ratios from data acquired with imaging spectrometers. Remote Sensing of Environment 43, 23–33.

Gower, S.T., Kucharik, C.J., Norman, J.M., 1999. Direct and indirect estimation of leaf area index f_{APAR}, and net primary production of terrestrial ecosystems. Remote Sensing of Environment 70, 29–51.

Halthore, R.N., Eck, T.F., Holben, B.N., Markham, B.L., 1997. Sun photometric measurements of atmospheric water vapor column abundance in the 940-nm band. Journal of Geophysical Research 102, 4343–4352.

Haboudane, D., Miller, J.R., Pattey, E., Zarco-Tejada, P.J., Strachan, I.B., 2004. Hyperspectral vegetation indices and novel algorithms for predicting green LAI of crop canopies: modeling and validation in the context of precision agriculture. Remote Sensing of Environment 90, 337–352.

Jacquemoud, S., Baret, F., 1990. PROSPECT: a model of leaf optical properties spectra. Remote Sensing of Environment 34, 75–91.

Jacquemoud, S., Baret, F., Andrieu, B., Danson, F.M., Jaggard, K., 1995. Extraction of vegetation biophysical parameters by inversion of the PROSPECT + SAIL model on sugar beet canopy reflectance data-application to TM data. Remote Sensing of Environment 52, 163–172.

Jacquemoud, S., Verhoef, W., Baret, F., Bacour, C., Zarco-Tejada, P.J., Asner, G.P., François, C., Ustin, S.L., 2009. PROSPECT + SAIL models: a review of use for vegetation characterization. Remote Sensing of Environment 113, S56–S66.

Kimes, D.S., Knyazikhin, Y., Privette, J.L., Abuelgasim, A.A., Gao, F., 2000. Inversion methods for physically-based models. Remote Sensing Reviews 18, 381–439.

Koetz, B., Baret, F., Poilvé, H., Hill, J., 2005. Use of coupled canopy structure dynamic and radiative transfer models to estimate biophysical canopy characteristics. Remote Sensing of Environment 95, 115–124.

Kuusk, A., 1995. A fast invertible canopy reflectance model. Remote Sensing of Environment 51, 342–350.

Li, Z.-L., Tang, R., Wan, Z., Bi, Y., Zhou, C., Tang, B., Yan, G., Zhang, X., 2009. A review of current methodologies for regional evapotranspiration estimation from remotely sensed data. Sensors 9, 3801–3853.

Li, Z.-L., Tang, B.-H., Wu, H., Ren, H., Yan, G., Wan, Z., Trigo, I.F., Sobrino, J.A., 2013a. Satellite-derived land surface temperature: current status and perspectives. Remote Sensing of Environment 131, 14–37.

Li, Z.-L., Wu, H., Wang, N., Qiu, S., Sobrino, J.A., Wan, Z., Tang, B.-H., Yan, G., 2013b. Land surface emissivity retrieval from satellite data. International Journal of Remote Sensing 34, 3084–3127.

Meroni, M., Colombo, R., Panigada, C., 2004. Inversion of a radiative transfer model with hyperspectral observations for LAI mapping in poplar plantations. Remote Sensing of Environment 92, 195–206.

Myneni, R.B., Hoffman, S., Knyazikhin, Y., Privette, J.L., Glassy, J., Tian, Y., Wang, Y., Song, X., Zhang, Y., Smith, G.R., Lotsch, A., Friedl, M., Morisette, J.T., Votava, P., Nemani, R.R., Running, S.W., 2002. Global products of vegetation leaf area and fraction absorbed PAR from year one of MODIS data. Remote Sensing of Environment 83, 214–231.

Richter, K., Atzberger, C., Vuolo, F., D'Urso, G., 2009. Experimental assessment of the Sentinel-2 band setting for RTM-based LAI retrieval of sugar beet and maize. Canadian Journal of Remote Sensing 35, 465–481.

Richter, K., Atzberger, C., Vuolo, F., D'Urso, G., 2011. Evaluation of Sentinel-2 spectral sampling for radiative transfer model based LAI estimation of wheat sugar beet, and maize. IEEE Journal of Selected Topics in Applied Earth Observations and Remote Sensing 4, 458–464.

Running, S.R., Baldocchi, D.D., Turner, D.P., Gower, S.T., Bakwin, P.S., Hibbard, K.A., 1999. A global terrestrial monitoring network integrating tower fluxes flask sampling, ecosystem modeling and EOS satellite data. Remote Sensing of Environment 70, 108–128.

Sandmeier, S., Müller, C., Hosgood, B., Andreoli, G., 1998. Physical mechanisms in hyperspectral BRDF data of grass and watercress. Remote Sensing of Environment 66, 222–233.

Schlerf, M., Atzberger, C., 2012. Vegetation structure retrieval in beech and spruce forests using spectrodirectional satellite data. IEEE Journal of Selected Topics in Applied Earth Observations and Remote Sensing 5, 8–17.

Si, Y., Schlerf, M., Zurita-Milla, R., Skidmore, A.K., Wang, T., 2012. Mapping the spatio-temporal variation of grassland quantity and quality using MERIS data and the PROSAIL model. Remote Sensing of Environment 121, 415–425.

Verhoef, W., 1984. Light scattering by leaf layers with application to canopy reflectance modeling: The SAIL model. Remote Sensing of Environment 16, 125–141.

Verhoef, W., 1985. Earth observation modeling based on layer scattering matrices. Remote Sensing of Environment 17, 165–178.

Verrelst, J., Romijn, E., Kooistra, L., 2012. Mapping vegetation density in a heterogeneous river floodplain ecosystem using pointable CHRIS/PROBA data. Remote Sensing 4, 2866–2889.

Vohland, M., Mader, S., Dorigo, W., 2010. Applying different inversion techniques to retrieve stand variables of summer barley with PROSPECT + SAIL. International Journal of Applied Earth Observation and Geoinformation 12, 71–80.

Vuolo, F., Dini, L., D'Urso, G., 2008. Retrieval of leaf area index from CHRIS/PROBA data: an analysis of the directional and spectral information content. International Journal of Remote Sensing 29, 5063–5072.

Weiss, M., Baret, F., Myneni, R.B., Pragnère, A., Knyazikhin, Y., 2000. Investigation of a model inversion technique to estimate canopy biophysical variables from spectral and directional reflectance data. Agronomie 20, 3–22.

Yang, F., Sun, J., Fang, H., Yao, Z., Zhang, J., Zhu, Y., Song, K., Wang, Z., Hu, M., 2012. Comparison of different methods for corn LAI estimation over northeastern China. International Journal of Applied Earth Observation and Geoinformation 18, 462–471.

Yang, G., Zhao, C., Liu, Q., Huang, W., Wang, J., 2011. Inversion of a radiative transfer model for estimating forest LAI from multisource and multiangular optical remote sensing data. IEEE Transactions on Geoscience and Remote Sensing 49, 988–1000.

Yao, Y., Liu, Q., Liu, Q., Li, X., 2008. LAI retrieval and uncertainty evaluations for typical row-planted crops at different growth stages. Remote Sensing of Environment 112, 94–106.

Zhao, F., Gu, X., Verhoef, W., Wang, Q., Yu, T., Liu, Q., Huang, H., Qin, W., Chen, L., Zhao, H., 2010. A spectral directional reflectance model of row crops. Remote Sensing of Environment 114, 265–285.